Int J Fract (2020) 222:13–23
https://doi.org/10.1007/s10704-020-00423-9

ORIGINAL PAPER

Tuning crack-inclusion interaction with an applied T-stress

Kai Guo · **Bo Ni** · **Huajian Gao**

Received: 18 August 2019 / Accepted: 16 January 2020 / Published online: 3 February 2020

Abstract The interaction between cracks and inclusions plays an important role in the fracture behavior of particulate composites. It is commonly recognized that an inclusion stiffer than the matrix tends to deflect an approaching crack away while a softer inclusion attracts the crack. Here, we demonstrate by analytical modeling and numerical simulations that the crack-inclusion interaction can be tuned by an applied T-stress. Under a sufficiently large compressive applied T-stress, cracks can be attracted to stiffer inclusions while repelled by softer ones, thus reversing the conventional trend. Potential applications of this work include composite electrodes in lithium-ion batteries and hydraulic fracturing.

Keywords Crack · Inclusion · Applied T-stress · Particulate composites

Kai Guo and Bo Ni contributed equally to this work.

Electronic supplementary material The online version of this article (https://doi.org/10.1007/s10704-020-00423-9) contains supplementary material, which is available to authorized users.

K. Guo · B. Ni · H. Gao (✉)
School of Engineering, Brown University, Providence, RI 02912, USA
e-mail: huajian_gao@brown.edu

K. Guo
Laboratory for Atomistic and Molecular Mechanics (LAMM), Department of Civil and Environmental Engineering, Massachusetts Institute of Technology, Cambridge, MA 02139, USA
e-mail: kaiguo@mit.edu

H. Gao
School of Mechanical and Aerospace Engineering, College of Engineering, Nanyang Technological University, 70 Nanyang Drive, Singapore 639798, Singapore

1 Introduction

Particulate composites are widely used in many engineering applications, ranging from structural composites to energy storage materials. The interaction between cracks and second phase particles (viz., inclusions with different elastic properties) has been extensively investigated. Analytical approaches have been developed to calculate the near-tip stress field, stress intensity factors (SIFs) and the configurational force for a crack in the vicinity of an inclusion (Atkinson 1972; Erdogan et al. 1974; Faber and Evans 1983a; Gdoutos 1985; Han and Chen 2000; Hwu et al. 1995; Li and Lv 2017; Li and Yang 2004; Rubinstein 1991; Sendeckyj 1974; Tamate 1968; Zhou and Li 2007; Zhou et al. 2011). Simulations using finite element method (FEM) have been performed to evaluate the SIF and energy release rate (ERR) for a stationary crack interacting with an inclusion (Haddi and Weichert 1998; Li and Chudnovsky 1993a, b; Lipetzky and Knesl 1995; Lipetzky and Schmauder 1994). In order to predict the trajectory and associated ERR of a propagating crack, various numerical techniques have been developed and applied, including boundary element method (BEM)

(Bush 1997; Kitey et al. 2006; Knight et al. 2002; Lei et al. 2005; Wang et al. 1998; Wang and Chau 2001), extended finite element method (XFEM) (Nielsen et al. 2012; Wang et al. 2012, 2015, 2018), element-free Galerkin (EFG) method (Muthu et al. 2013, 2016) and cohesive zone type models (CZM) (Ponnusami et al. 2015). Advances in experimental techniques have also allowed direct observation of crack trajectory in particulate composites (Chudnovsky et al. 1987; Faber and Evans 1983b; Kitey and Tippur 2005a, b, 2008).

A widely known conclusion from existing studies is that a stiff, well-bonded inclusion tends to reduce the SIF of an approaching mode I crack and deflect it away, while a soft or debonded inclusion tends to attract a crack (Bush 1997; Erdogan et al. 1974; Kitey et al. 2006; Knight et al. 2002; Lei et al. 2005; Muthu et al. 2013; Wang et al. 1998, 2012; Zhou et al. 2011). However, one might note that this conclusion has been primarily drawn from the behavior of the singular stress field near the crack tip, i.e. the K-field. On the other hand, it is also known that the constant term in the Williams expansion of the crack tip field (Williams 1957), the so-called T-stress which acts in parallel to the crack, can strongly influence the propagation path of a mode I crack (Cotterell 1966; Cotterell and Rice 1980; Gupta et al. 2015). So far, the effect of T-stress on crack-inclusion interaction has only been discussed in a few studies in the literature. For example, Han and Chen (2000) showed that T-stress can influence the SIFs of an interfacial crack in the vicinity of a microvoid using a 'psuedo-traction-edge-dislocation' method. Zhou and Li (2007) found that T-stress has a shielding (or amplification) effect on the mode I SIF (K_I) during crack-inclusion interaction. Wang et al. (2018) presented an interaction integral method combined with XFEM to evaluate the SIFs and T-stress for a center crack in the vicinity of an inclusion subject to far field tension, including the effect of the inclusion on T-stress at the crack tip. In their model, the T-stress is influenced by a remote loading acting normal to the crack as well as the inclusion. In many engineering applications, an applied stress/loading parallel to the crack plane can alter the T-stress, which will be referred to in this paper as an applied T-stress, T^{app}, in order to distinguish it from the T-stress at the crack tip. To the best of our knowledge, the effect of T^{app} on the trajectory of a crack in the vicinity of an inclusion has not been investigated, even though it could be critical to the reliability and performance of not only conventional particle reinforced composites but also many other particulate composite systems. For instance, composite electrodes in lithium-ion batteries (Fig. 1a) undergo substantial compressive stresses due to Li intercalation into active materials (Hassoun et al. 2008; Kumar et al. 2017; Obrovac and Chevrier 2015). The attraction between cracks and active material particles can induce capacity fade through loss of contact between the matrix and active materials. In addition, hydraulic fracturing designed for stimulating unconventional reservoirs (e.g., tight gas and shale) has attracted interests from the oil and gas industry in recent years (Barati and Liang 2014). Underground shales (Fig. 1b) naturally undergo a triaxial compressive loading (Gomez and He 2006; Gramberg 1965), resulting in significant T-stress during the fracturing process. The T-effect on crack-inclusion interaction can play a crucial role in promoting/suppressing crack networks in connecting rock pores which store natural gas, affecting overall gas production.

The present work is aimed to investigate the effect of an applied T-stress on the trajectory of a crack in the vicinity of an inclusion. Through an integrated theoretical and numerical approach, we will demonstrate that a sufficiently large compressive applied T-stress can fundamentally change the interaction between cracks and inclusions in particulate composites.

2 Theoretical analysis

In many engineering applications, the geometry and loading condition involving crack-inclusion interaction could be very complicated. Without loss of generality, the present work focuses on the universal feature of crack tip fields and studies the model problem of an semi-infinite edge crack in a two dimensional (2D) plane-strain elastic medium subjected to a mode I SIF, K_I^{∞} as well as an applied T-stress, T^{app}. According to linear elastic fracture mechanics (LEFM), the stress field, $\boldsymbol{\sigma}^A(r,\theta)$, around the crack tip under such loading reads,

$$\begin{cases} \sigma_{11}^A(r,\theta) = \frac{K_I^{\infty}}{\sqrt{2\pi r}}\left(1-\sin\frac{\theta}{2}\sin\frac{3\theta}{2}\right)\cos\frac{\theta}{2} + T^{app}, \\ \sigma_{22}^A(r,\theta) = \frac{K_I^{\infty}}{\sqrt{2\pi r}}\left(1+\sin\frac{\theta}{2}\sin\frac{3\theta}{2}\right)\cos\frac{\theta}{2}, \\ \sigma_{12}^A(r,\theta) = \frac{K_I^{\infty}}{\sqrt{2\pi r}}\cos\frac{\theta}{2}\sin\frac{\theta}{2}\cos\frac{3\theta}{2}. \end{cases} \tag{1}$$

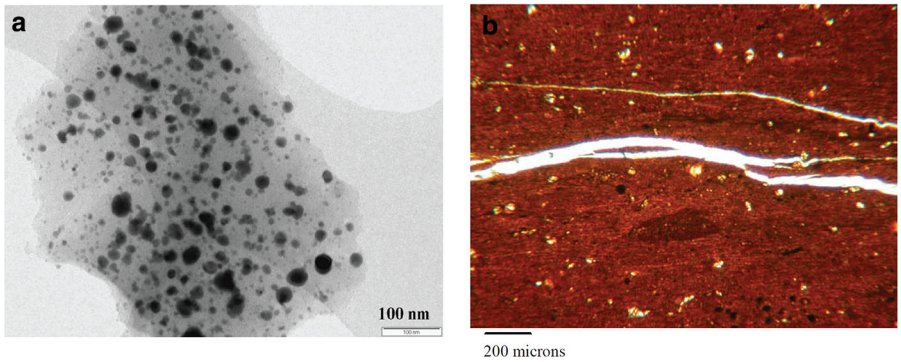

Fig. 1 **a** TEM image of a Sn–C nanocomposite electrode in lithium batteries (reprinted from Hassoun et al. (2008) with permission from Wiley-VCH STM Copyright); **b** fractures in Nahr Umr shale (Gomez and He 2006)

The corresponding strain field is,

$$\begin{cases} \varepsilon_{11}^{A}(r,\theta)=\frac{K_I^{\infty}}{2\mu^M\sqrt{2\pi r}}\left(1-2\nu^M-\sin\frac{\theta}{2}\sin\frac{3\theta}{2}\right)\cos\frac{\theta}{2}+\frac{1-\nu^M}{2\mu^M}T^{app}, \\ \varepsilon_{22}^{A}(r,\theta)=\frac{K_I^{\infty}}{2\mu^M\sqrt{2\pi r}}\left(1-2\nu^M+\sin\frac{\theta}{2}\sin\frac{3\theta}{2}\right)\cos\frac{\theta}{2}-\frac{\nu^M}{2\mu^M}T^{app}, \\ \varepsilon_{12}^{A}(r,\theta)=\frac{K_I^{\infty}}{2\mu^M\sqrt{2\pi r}}\cos\frac{\theta}{2}\sin\frac{\theta}{2}\cos\frac{3\theta}{2}. \end{cases} \tag{2}$$

where μ^M and ν^M are the shear modulus and Poisson's ratio of the matrix material, (r,θ) are the polar coordinates originated at the crack tip and the crack lies along $\theta=-\pi$.

To consider the effect of inclusion, assume there exists an inclusion with different elastic properties (μ^I,ν^I) located at position (r^I,θ^I), as illustrated in Fig. 2a. We aim at estimating the potential energy change due to the creation of such an inclusion. For simplicity, here the inclusion is assumed to be circular with a relatively small radius of R, i.e., $R\ll r^I$. Under such conditions, the stress/strain fields in Eqs. (1) and (2) are expected to be approximately valid everywhere except in the vicinity of the inclusion. Near the inclusion, the problem could be treated as an Eshelby inhomogeneity subjected to a remote loading, $\boldsymbol{\sigma}^A(r^I,\theta^I)$. Based on Eshelby's equivalent inclusion theory (Eshelby 1957), the equivalent transformation strain in the inclusion takes the following form,

$$\begin{cases} \boldsymbol{\varepsilon}^T=\mathbf{L}\boldsymbol{\varepsilon}^A(r^I,\theta^I), \\ \mathbf{L}=[(\mathbf{C}^I-\mathbf{C}^M)\mathbf{S}+\mathbf{C}^M]^{-1}(\mathbf{C}^M-\mathbf{C}^I), \end{cases} \tag{3}$$

where $\mathbf{S}$ is the Eshelby tensor, $\mathbf{C}^I$ and $\mathbf{C}^M$ are the elastic stiffness tensors of the inclusion and matrix. For simplicity, we assume both the matrix and inclusion materials are isotropic and share the same Poisson's ratio, ν, and we write,

$$\mathbf{C}^I=\alpha\,\mathbf{C}^M. \tag{4}$$

where $\alpha=\mu^I/\mu^M$ is the non-dimensional stiffness of the inclusion. For circular inclusions, the Eshelby tensor is constant (Mura 1987), and the non-trivial components of the $\mathbf{L}$ tensor in Eq. (3) can be expressed as (Li and Yang 2004; Zhou et al. 2011),

$$\begin{aligned} L_{1111}&=L_{2222}=\frac{(1-\alpha)(1-\nu)(3-4\nu+5\alpha-4\nu\alpha)}{(1+\alpha-2\nu)(1+3\alpha-4\nu\alpha)}, \\ L_{1122}&=L_{2211}=-\frac{(1-\alpha)^2(1-\nu)(1-4\nu)}{(1+\alpha-2\nu)(1+3\alpha-4\nu\alpha)}, \\ L_{1133}&=L_{2233}=\frac{(1-\alpha)^2\nu}{(1+\alpha-2\nu)},\quad L_{3333}=1-\alpha, \\ L_{1212}&=\frac{4(1-\alpha)(1-\nu)}{(1+3\alpha-4\nu\alpha)},\quad L_{1313}=L_{2323}=\frac{2(1-\alpha)}{1+\alpha}. \end{aligned} \tag{5}$$

The potential energy change associated with the creation of such an inclusion is given by (Eshelby 1957),

$$\Delta U^I=-\frac{\pi R^2}{2}\boldsymbol{\sigma}^A(r^I,\theta^I):\boldsymbol{\varepsilon}^T(r^I,\theta^I). \tag{6}$$

Note that ΔU^I explicitly depends on the location of the inclusion, (r^I,θ^I), due to the non-uniform stress/strain fields, $(\boldsymbol{\sigma}^A,\boldsymbol{\varepsilon}^A)$, around the crack tip. Recall that the J-integral vector, (J_1,J_2), measures the potential energy release rate due to the translational shift of defects such as cracks and inclusions, also known as the configurational force or material force. Thus, the J-integral vector along a contour Γ^I that encloses only the inclusion in Fig. 2b can be calculated as,

$$J_i^I=-\frac{\partial(\Delta U^I)}{\partial x_i^I},\quad i=1,2. \tag{7}$$

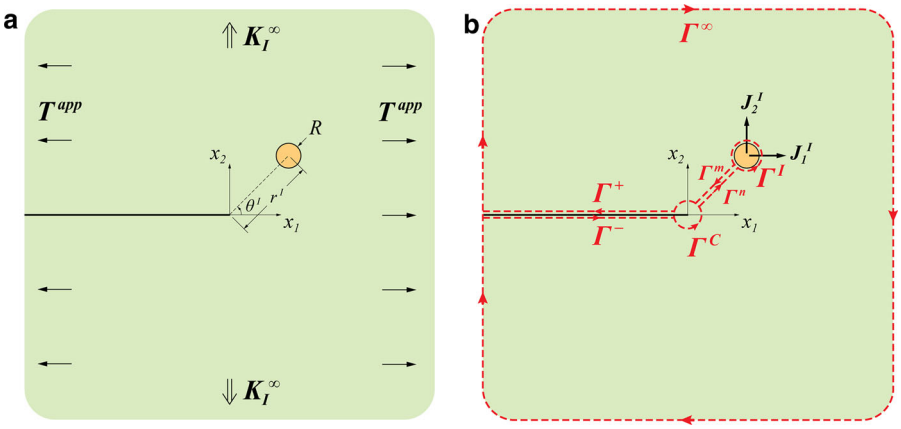

Fig. 2 **a** Geometry and boundary conditions in the crack-inclusion problem under investigation. **b** Paths of contour integrals

where $x_i^I, i = 1, 2$ are Cartesian coordinates of the inclusion. Combining Eqs. (1), (3), (6) and (7) yields an explicit expression for the J-integral vector of the inclusion,

$$J_1^I = -J_1^\infty \left[\frac{1}{\rho^2} f_1(\theta^I, \alpha, \nu) + \frac{\beta}{\rho\sqrt{\rho}} g_1(\theta^I, \alpha, \nu) \right], \tag{8}$$

$$J_2^I = -J_1^\infty \left[\frac{1}{\rho^2} f_2(\theta^I, \alpha, \nu) + \frac{\beta}{\rho\sqrt{\rho}} g_2(\theta^I, \alpha, \nu) \right], \tag{9}$$

where $J_1^\infty = (1-\nu^M)(K_I^\infty)^2/2\mu^M$ is the J_1 integral around the crack tip without the presence of the inclusion; $\rho = r^I/R$ is a normalized distance between the crack tip and inclusion; $\beta = \sqrt{\pi R} T^{app}/K_I^\infty$ is a normalized applied T-stress; $f_i(\theta^I, \alpha, \nu)$ and $g_i(\theta^I, \alpha, \nu)$, for $i = 1, 2$, show the dependence on the inclusion orientation θ^I and material properties (α, ν), as the following,

$$\begin{aligned}
f_1(\theta^I, \alpha, \nu) &= C_1 \cos\frac{\theta^I}{2}\cos\frac{3\theta^I}{2} + 3C_2 \sin^2\theta^I \cos\theta^I, \\
g_1(\theta^I, \alpha, \nu) &= \frac{1}{\sqrt{2}} \begin{pmatrix} -C_2 \cos\frac{3}{2}\theta^I + 3C_2 \cos\frac{7}{2}\theta^I \\ +C_1 C_2 \frac{4\alpha}{1-\alpha} \frac{(1-\nu)(1-4\nu)}{1-2\nu} \cos\frac{3}{2}\theta^I \end{pmatrix}, \\
f_2(\theta^I, \alpha, \nu) &= \frac{1}{2} \begin{pmatrix} C_1 \sin\theta^I + C_1 \sin 2\theta^I - 3C_2 \sin\theta^I \\ -5C_2 \sin\theta^I \cos 2\theta^I + 4C_2 \cos^2\theta^I \sin\theta^I \end{pmatrix}, \\
g_2(\theta^I, \alpha, \nu) &= \frac{1}{\sqrt{2}} \begin{pmatrix} 3C_2 \sin\frac{3}{2}\theta^I + 3C_2 \sin\frac{7}{2}\theta^I \\ +C_1 C_2 \frac{4\alpha}{1-\alpha} \frac{(1-\nu)(1-4\nu)}{1-2\nu} \sin\frac{3}{2}\theta^I \end{pmatrix},
\end{aligned} \tag{10}$$

where

$$C_1 = \frac{(1-\alpha)(1-2\nu)}{(1+\alpha-2\nu)}, C_2 = \frac{(1-\alpha)}{2(1+3\alpha-4\alpha\nu)}. \tag{11}$$

In Eqs. (8) and (9), the first terms in the brackets represent the interaction solely between the crack tip and the inclusion while the second terms result from the three-party interaction between the crack tip, the inclusion and the applied T-stress. It should be noted that the former scales with the normalized crack-inclusion distance as ρ^{-2} while the latter as $\rho^{-3/2}$ for $\rho > 1$. Next, we estimate the local SIFs at the crack tip in the presence of the inclusion and the applied T-stress.

To connect J-integrals at the crack and the inclusion, in addition to the inclusion contour, Γ^I, the following contours and paths are constructed (Fig. 2b): Γ^C, an infinitesimal circular contour surrounding the crack tip; Γ^∞, an infinite large contour enclosing both the crack and the inclusion; Γ^+ and Γ^-, line paths along the upper and lower crack surfaces connecting the infinite contour Γ^∞ and the crack tip contour Γ^C; Γ^m and Γ^n, line paths that connect the crack tip contour Γ^C and the inclusion contour Γ^I and are infinitely close to each other. The combined path, $\Gamma^\infty \cup \Gamma^C \cup \Gamma^I \cup \Gamma^m \cup \Gamma^n \cup \Gamma^+ \cup \Gamma^-$, with the marked directions in Fig. 2b, encloses a simply connected region of matrix material containing no singularities or defects. So, the J-integral vector vanishes along this path, i.e.,

$$\begin{aligned}
&J_i^C + J_i^I + J_i|_{\Gamma^m} + J_i|_{\Gamma^n} \\
&\quad + J_i|_{\Gamma^+} + J_i|_{\Gamma^-} + J_i|_{\Gamma^\infty} = 0, \ i = 1, 2
\end{aligned} \tag{12}$$

where $J_i = \int_\Gamma (w n_i - \sigma_{kj} n_k \frac{\partial u_j}{\partial x_i}) \, \mathrm{d}\Gamma$, w is the strain energy density, n_k the components of the unit nor-

mal vector along the path, σ_{kj} and u_j the stress and displacement components, respectively, $J_i^C = \lim_{r\to 0}\int_{-\pi}^{\pi}(wn_i - \sigma_{kj}n_k\frac{\partial u_j}{\partial x_i})rd\theta$ is the J-integral along an infinitesimal circular path,[1] Γ^C, surrounding the crack tip. As the paths Γ^m and Γ^n approach each other, it is straightforward to show that $J_i|_{\Gamma^m} + J_i|_{\Gamma^n} = 0$. Using the stress/strain field in Eqs. (1) and (2) as an approximation to the real stress/strain field and plugging it into the J-integral definition, we have $J_i|_{\Gamma^+} + J_i|_{\Gamma^-} = 0$.[2] Along the infinite contour Γ^∞ where the effect of inclusion becomes "invisible", we have $J_1|_{\Gamma^\infty} = -J_1^\infty$ and $J_2|_{\Gamma^\infty} = 0$, where $J_1^\infty = (1-\nu^M)(K_I^\infty)^2/2\mu^M$ is the J_1 integral around the crack tip without the presence of the inclusion. Therefore, Eq. (12) can be reduced to,

$$\begin{cases} J_1^C = J_1^\infty - J_1^I \\ J_2^C = -J_2^I \end{cases} . \tag{13}$$

Inserting Eqs. (8) and (9) into Eq. (13), we have the J-integral at the crack tip in the presence of the inclusion and the applied T-stress,

$$\begin{cases} J_1^C = J_1^\infty \left[1 + \frac{1}{\rho^2} f_1(\theta^I, \alpha, \nu) + \frac{\beta}{\rho\sqrt{\rho}} g_1(\theta^I, \alpha, \nu)\right] \\ J_2^C = J_1^\infty \left[\frac{1}{\rho^2} f_2(\theta^I, \alpha, \nu) + \frac{\beta}{\rho\sqrt{\rho}} g_2(\theta^I, \alpha, \nu)\right] \end{cases} . \tag{14}$$

Recall that the J-integral and the SIFs (K_I, K_{II}) at the crack tip have the following relation,

$$\begin{aligned} J_1^C &= \frac{1-\nu^M}{2\mu^M}\left[(K_I)^2 + (K_{II})^2\right], \\ J_2^C &= -\frac{1-\nu^M}{\mu^M} K_I K_{II} . \end{aligned} \tag{15}$$

Combining Eqs. (14) and (15), it is straightforward to calculate the SIFs in the presence of the inclusion as well as the applied T-stress.

To further demonstrate the physical implication of the solution, let us focus on the initial stage of a crack approaching the inclusion, i.e., when the normalized distance between the crack tip and inclusion is still relatively large, i.e., $\rho \gg 1$. According to Eqs. (8) and (9), we have $|J_1^\infty| \gg |J_1^I|, |J_2^I|$ and thus Eq. (13) can be approximated as

$$\begin{cases} J_1^C \approx J_1^\infty \\ J_2^C = -J_2^I \end{cases} . \tag{16}$$

With the aids of Eqs. (15), (16), we can derive the mode II SIF of the crack under the presence of the inclusion and the applied T-stress explicitly as,

$$K_{II} \approx \frac{\mu^M}{(1-\nu)K_I^\infty} J_2^I . \tag{17}$$

It is generally accepted that the deflection of a crack is mainly governed by the mode II SIF, K_{II} (Cotterell and Rice 1980). For example, considering a crack approaching an inclusion above the prospective crack path (i.e., $0 < \theta^I < 90°$), Eq. (17) above implies that the repelling configurational force between the inclusion and crack in the vertical direction (i.e., $J_2^I > 0$) tends to deflect the crack away from the inclusion (i.e., $K_{II} > 0$), while an attractive configurational force is likely to deflect the crack path towards the inclusion. It is important to note that the configurational force on the inclusion depends on not only the inclusion but also the applied T-stress. Equations (8), (9), (14), (16) and (17) are the main results of the theoretical model and will be further discussed in Sect. 4.

3 Numerical simulations

3.1 FEM calculations for SIF

In order to validate the results from our theoretical analysis, FEM simulations were performed in a 2D, plane strain, square domain of length L, as illustrated in Fig. S1. The domain consists of a straight edge crack of length a with its tip located at the center of the domain (i.e., $a = L/2$) and a circular inclusion of radius R embedded at the matrix at a distance r^I from the crack tip and an angle θ^I from the reference axis x_1. As the theoretical analysis considers an infinite medium, the size of the FEM domain is sufficiently large by taking $L/r^I = 50$ to reduce the boundary effect. The superposition of the applied K_I^∞ and T^{app} is achieved by applying displacement boundary conditions to the

[1] This infinitesimal contour limit is required by the definition of J_2 while it is not for J_1.

[2] It should be emphasized that for J_2, $J_2|_{\Gamma^+} + J_2|_{\Gamma^-} = \int_{-\infty}^{0}(w^+ - w^-)\,dx_1$ is not necessarily equal to zero even through it is well known that J_1 integral vanishes along Γ^+ and Γ^- (Eischen 1987; Herrmann and Herrmann 1981).

FEM domain (see Fig. S1). For K_I^∞, the components of the displacement are given by the following equations (Bower 2010),

$$\begin{cases} u_1 = \frac{K_I^\infty}{\mu^M}\sqrt{\frac{r}{2\pi}}\left[1-2\nu^M+\sin^2\frac{\theta}{2}\right]\cos\frac{\theta}{2} \\ u_2 = \frac{K_I^\infty}{\mu^M}\sqrt{\frac{r}{2\pi}}\left[2-2\nu^M-\cos^2\frac{\theta}{2}\right]\sin\frac{\theta}{2} \end{cases}, \tag{18}$$

where r and θ are polar coordinates along the boundary of the domain. The displacements corresponding to the applied T-stress are

$$\begin{cases} u_1 = \frac{1-\nu^M}{2\mu^M}T^{app}x_1 \\ u_2 = \frac{-\nu^M}{2\mu^M}T^{app}x_2 \end{cases}, \tag{19}$$

where x_1 and x_2 are Cartesian coordinates along the boundary. In the FEM model, combined displacement boundary conditions given in Eqs. (18) and (19) are applied. The interaction integral method provided by the commercial software ABAQUS (Dassault Systemes Simulia Corp., Providence, RI) was adopted to calculate the SIFs of the crack, with 8-noded biquadratic plane strain quadrilateral elements (CPE8R) assigned to the entire mesh.

3.2 Extended FEM model for crack trajectory prediction

The analytical model in Sect. 2 that yields explicit expressions of SIFs is based on the configuration of a straight crack interacting with an inclusion. However, it is likely that a propagating crack starts to deflect when it is still far away from the inclusion. In order to capture the crack propagation trajectory, we implemented an extended finite element method (XFEM) (Belytschko and Black 1999; Daux et al. 2000; Moes et al. 1999) in ABAQUS with the maximum principal stress criterion. The details of the XFEM model will be discussed in Sect. 4.3.

4 Results and discussions

The effect of an applied T-stress on the crack-inclusion interaction results from a three-party interaction involving the crack, the inclusion and the applied T-stress, and can be influenced by varying combinations of material properties, defect positions and loading conditions in different engineering problems. To validate and elaborate the theoretical and numerical results and their implications, the main results are addressed and discussed in the following.

4.1 Driving force on the crack tip

a. In the absence of an inclusion, i.e. $\alpha = 1$, Eqs. (8) and (9) show that the configurational force between the crack tip and the inclusion vanishes. Thus, the driving force and SIFs at the crack tip are independent of the applied T-stress, as expected.
b. Without the applied T-stress, the presence of the inclusion can still affect the driving force at the crack tip. Letting the normalized applied T-stress vanish, i.e., $\beta = 0$, in Eq (14), one obtains the driving force at the crack tip as

$$\begin{cases} J_1^C = J_1^\infty\left[1+\frac{1}{\rho^2}f_1^I(\theta^I,\alpha,\nu)\right] \\ J_2^C = J_1^\infty\left[\frac{1}{\rho^2}f_2^I(\theta^I,\alpha,\nu)\right] \end{cases}. \tag{20}$$

which are in agreement with the previous reported results (Li and Lv 2017).[3] Correspondingly, the change in crack tip driving force, $J_i^C - J_i^\infty, i = 1, 2$, induced by the crack-inclusion (C-I) interaction are

$$\Delta J_i^C|_{\text{C-I}} = J_1^\infty\frac{1}{\rho^2}f_i(\theta^I,\alpha,\nu), \quad i=1,2 \tag{21}$$

which scales with the normalized crack-inclusion distance as ρ^{-2} for $\rho > 1$.
In the special case of $\theta^I = 0$, i.e., for the inclusion sitting right ahead of the crack tip, Eq. (20) reduces to

$$\begin{cases} J_1^C = J_1^\infty\left[1+\frac{1}{\rho^2}\frac{(1-\alpha)(1-2\nu)}{(1+\alpha-2\nu)}\right] \\ J_2^C = 0 \end{cases}. \tag{22}$$

In this case, a softer inclusion (i.e. $0 \leqslant \alpha < 1$) amplifies the crack tip driving force (i.e. $J_1^C/J_1^\infty > 1$) while a stiffer inclusion (i.e. $\alpha > 1$) has a shielding effect on the crack (i.e. $J_1^C/J_1^\infty < 1$). More generally, Eq. (20) predicts that a softer/stiffer inclusion tends to attract/repel the crack.

[3] It should be noted that the counterpart of J_2^C obtained in (Li and Lv 2017) misses one term compared to our results due to possible mistakes in derivation.

c. In the presence of an inclusion, an applied T-stress provides an effective way to tune the crack-inclusion interaction. Comparing Eq. (14) with Eq. (20), one can see that the applied T-stress alters the crack tip driving force by the following crack-inclusion-T-stress (C-I-T) interaction terms

$$\Delta J_i^C|_{\text{C-I-}T} = J_1^\infty \frac{\beta}{\rho\sqrt{\rho}} g_i(\theta^I, \alpha, \nu), \quad i = 1, 2 \tag{23}$$

which scale with the normalized crack-inclusion distance as $\rho^{-3/2}$, in proportion to the normalized applied T-stress β, and also depend on the elastic properties of the inclusion.
Comparing Eqs. (21) and (23), it is important to note that the scaling of the T-effect terms in Eq. (23) decays slower than that of the solo influence of the inclusion in Eq. (21) for $\rho > 1$. Consequently, by choosing a proper applied T-stress, there exists the possibility for the applied T-stress to compete with, and even overcome the solo effect of the inclusion, which provides a pathway to tune the crack-inclusion interaction.

To validate the theoretical predictions and demonstrate this capability of tuning crack-inclusion interaction via the applied T-stress, we performed FEM simulations to calculate and compare the SIFs of the crack tip under the presence of varying inclusion and applied T-stress in the next section.

4.2 SIF calculations

Without loss of generality, consider a crack approaching an inclusion above the prospective crack path (i.e., $0 < \theta^I < 90°$). As the deflection of a crack is governed by mode II SIF (Cotterell and Rice 1980), we consider normalized $\overline{K}_{II}$,

$$\overline{K}_{II} = \frac{2K_{II}(1-\nu)}{K_I^\infty}, \tag{24}$$

as an indicator of attraction or repulsion between a crack and inclusion. A positive $\overline{K}_{II}$ indicates that the crack deflects downwards and thus is repelled by the inclusion, while a negative $\overline{K}_{II}$ indicates that the crack will propagate upwards due to the attraction of the inclusion.

Figure 3 plots the variations of $\overline{K}_{II}$ as a function of θ^I with different dimensionless parameters $\alpha = \mu^I/\mu^M$ and $\beta = T^{app}\sqrt{\pi R}/K_I^\infty$ that represent the relative stiffness of the inclusion and the normalized applied T-stress, respectively. If the inclusion is stiffer than the matrix ($\alpha = 3$), as shown in Fig. 3a, it repels the crack subject to a pure K_I^∞ loading without applied T-stress ($\beta = 0$), but surprisingly it is found that in the presence of a sufficiently large compressive applied T-stress ($\beta = -1/3$) the stiffer inclusion strongly attracts the crack when $0 < \theta^I < 60°$. Figure 3b shows that the crack is attracted towards the softer inclusion ($\alpha = 1/3$) without an applied T-stress while deflected away from the inclusion under a compressive T-stress when $0 < \theta^I < 60°$. In addition, higher magnitude of β enhances the magnitude of $\overline{K}_{II}$, as shown in Fig. S2. In this regard, by applying a sufficiently large far field compressive T-stress, the conventional interaction trend between a propagating crack and an inclusion can be fundamentally changed, i.e., from attraction to repulsion and vice versa. Fig. 3 also shows that a tensile T^{app} ($\beta = 1/3$) keeps the same trend but amplifies the attraction or repulsion effect in the absence of T^{app} when $0 < \theta^I < 60°$. FEM results with $r^I/R = 10$ (dots in Fig. 3) show good agreement with the analytical solution obtained under assumption $R \ll r^I$. It is also shown that the discrepancy between analytical predictions and FEM simulations rises as r^I/R decreases, but the analytical solution still provides an acceptable estimate of $\overline{K}_{II}$ even in the case of $r^I/R = 2$ (see Fig. S3).

4.3 Crack trajectory near an inclusion under an applied T-stress

Figure 4a illustrates the adopted XFEM model, as a plane strain square domain of length L, consisting a pre-existing edge crack of length a and a circular inclusion of radius R located at an offset from the prospective crack path by a distance d. The chosen geometric parameters ($R/L = 0.05$, $a/L = 0.1$ and $d/R = 1$) and mesh size ensure that the calculated crack trajectory is not sensitive to the domain size, initial crack length or mesh. The shear modulus ratio between the inclusion and matrix is taken to be $\alpha = 10$ (a stiffer inclusion) or $\alpha = 0.1$ (a softer inclusion). The Poisson's ratios of the two phases are assumed to be identical ($\nu^I = \nu^M = 0.33$). The domain is subject to a

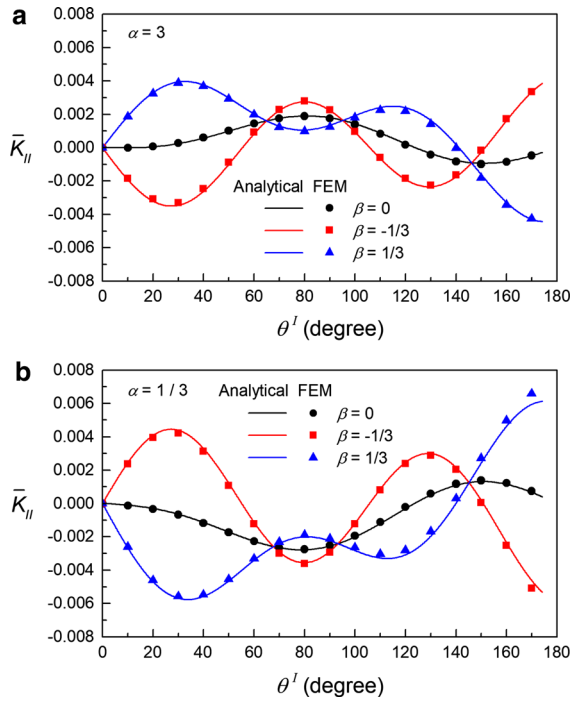

Fig. 3 Normalized mode II SIF as a function of θ^I for different values of parameter β for a crack interacting with an inclusion **a** stiffer ($\alpha = 3$) or **b** softer ($\alpha = 1/3$) than the matrix. The distance between the crack tip and inclusion center is fixed at $r^I = 10R$. The solid lines correspond to the analytical solution and the dots are FEM results

biaxial loading: uniform tensile stress acting normal to the crack plane (σ_y in Fig. 4a) and uniform normal stress acting parallel to the crack (σ_x in Fig. 4a). To study the T-effect, two different loadings, $\sigma_x = 0$ and $\sigma_x = -3\sigma_y$, were applied for comparison. It should be pointed out that even for a homogeneous square domain ($\alpha = 1$) under uniaxial tension (i.e., $\sigma_x = 0$), the T-stress at the crack tip is non-zero and varies with the crack length, from about $-0.53\sigma_y$ at $a/L = 0.1$ to about $0.63\sigma_y$ at $a/L = 0.5$ (Sherry et al. 1995). In this regard, the normalized applied T-stress β varies from -0.32 at $a/L = 0.1$ to 0.16 at $a/L = 0.5$ when $\sigma_x = 0$, and from -2.1 at $a/L = 0.1$ to -0.59 at $a/L = 0.5$ when $\sigma_x = -3\sigma_y$. Thus, the crack in the latter case experiences a much higher compressive T-stress than in the former case.

The crack trajectories in the vicinity of the inclusion under uniaxial tension ($\sigma_x = 0$) are shown in Fig. 4b. The stiffer inclusion deflects the approaching crack away while the softer inclusion attracts the crack, similar to the trend reported in previous studies (Muthu et al. 2013; Wang et al. 2012). Interestingly, when the compressive loading acting parallel to the crack is applied ($\sigma_x = -3\sigma_y$), Fig. 4c shows that the crack is attracted by the stiffer inclusion while repelled by the softer one, suggesting that the trend of crack-inclusion interaction has been reversed.

Comparison of Figs. 3 and 4 demonstrates that the variations of mode II SIF from the analytical solution is in qualitative agreement with the simulated crack trajectory by XFEM. For a crack in the vicinity of the softer inclusion under a compressive applied T-stress, the mode II SIF (red line in Fig. 3b) is positive when $0 < \theta^I < 60°$, turns negative when $60° < \theta^I < 100°$, and becomes positive again when $100° < \theta^I < 150°$, which is consistent with the crack trajectory (red solid line in Fig. 4c) where the vertical distance between the crack and inclusion initially increases, then decreases around the top region of the inclusion, and increases and decreases again as the crack propagates away from the inclusion. Another observation is that the crack does not deflect until it is about one radius away from the inclusion-matrix interface in the absence of σ_x in Fig. 4b; while if the compressive σ_x is applied, significant deflection occurs when the crack is about three radii away from the inclusion, as shown in Fig. 4c. This is in agreement with the SIF plots in Fig. 3 and Fig. S2 where the magnitude of $\overline{K}_{II}$ in the presence of sufficiently large compressive T-stress ($\beta < -1/3$) is higher than that in the absence of T-stress as the crack approaches the inclusion ($0 < \theta^I < 60°$). Both SIF calculations and XFEM simulations thus support the conclusion that a sufficiently large compressive applied T-stress can reverse the conventional trend of crack-inclusion interaction.

5 Conclusion

For particulate composites subject to uniaxial tension, it is widely known that an inclusion well-bonded to and stiffer/softer than a matrix tends to repel/attract an approaching crack. In the present work, we have presented an integrated theoretical and numerical study on the effect of an applied T-stress on crack–inclusion interaction. Our analytical solution and finite element results both suggest that a sufficiently large compressive applied T-stress can reverse the above conventional trend of crack–inclusion interaction, in the sense that the applied T can render the crack attracted toward

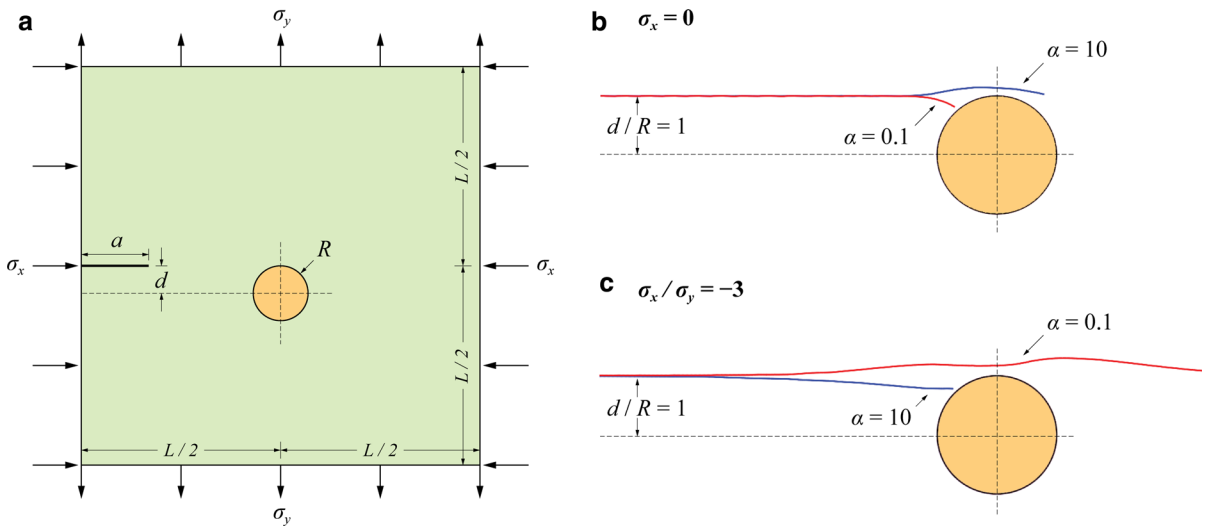

Fig. 4 **a** Initial configuration and boundary conditions of XFEM simulations. XFEM simulated crack paths in the vicinity of a stiffer inclusion ($\alpha = 10$) or softer inclusion ($\alpha = 0.1$) with **b** $\sigma_x = 0$ and **c** $\sigma_x/\sigma_y = -3$

a stiffer inclusion and repelled away from a softer inclusion. This T-effect on crack-inclusion interaction is potentially important for the following particulate composite systems.

- For particle reinforced composites, previous studies have shown that stiff and tough particles in a compliant matrix with strong interfacial bonding can toughen the material if crack arrest occurs (Wang et al. 1998). In this regard, applying a large compressive loading parallel to the crack plane could be a strategy to facilitate crack arrest as the repulsion between the cracks and stiff particles turns into attraction.
- Composite electrodes used in commercial lithium-ion batteries are typically particulate composites where active material particles are embedded in a matrix that consists of binders, conductive materials, pores, etc. Lithium intercalation into high capacity active materials such as silicon can induce substantial compressive stress in the electrodes. Thus, cracks propagating in the matrix would be attracted towards the stiff active particles, which could further induce capacity fade through the detachment of the active material particles from the conductive matrix.
- Rock pores in underground shales, which trap natural gas, can be seen as inclusions with zero stiffness (i.e., voids) in a stiff matrix. In the field of hydraulic fracturing, the induced fracture network is expected to pass through as many rock pores as possible. High compressive T-stress for hydraulic fractures might cause repulsion between the pores and induced cracks. Due to the gravity effect, underground shales undergo a triaxial differential compressive loading and the major compressive principle stress is usually along the vertical direction, so horizontal hydraulic fractures are likely to provide higher gas production by passing through more rock pores in comparison with vertical fractures.

Depending on the application that a particulate composite is designed for, attraction (or repulsion) between cracks and inclusions is probably desirable in some particulate composites, while should be avoided in some others. The present work suggests a strategy to tune crack-inclusion interaction with an applied T-stress, which may shed some light on the design of particulate composites with improved reliability and performance.

Acknowledgements The authors acknowledge the support by the Assistant Secretary for Energy Efficiency and Renewable Energy, Vehicle Technologies Office of the U.S. Department of Energy under Contract No. Award Number DE-EE0007787 under the Battery Material Research (BMR) Program and the National Science Foundation under grant CMMI-1634492.

References

Atkinson C (1972) Interaction between a crack and an inclusion. Int J Eng Sci 10:127–136

Barati R, Liang JT (2014) A review of fracturing fluid systems used for hydraulic fracturing of oil and gas wells. J Appl Polym Sci 131:40735

Belytschko T, Black T (1999) Elastic crack growth in finite elements with minimal remeshing. Int J Numer Methods Eng 45:601–620

Bower AF (2010) Applied mechanics of solids. CRC Press, Boca Raton

Bush MB (1997) The interaction between a crack and a particle cluster. Int J Fract 88:215–232

Chudnovsky A, Chaoui K, Moet A (1987) Curvilinear crack layer propagation. J Mater Sci Lett 6:1033–1038

Cotterell B (1966) Notes on paths and stability of cracks. Int J Fract Mech 2:526–533

Cotterell B, Rice JR (1980) Slightly curved or kinked cracks. Int J Fract 16:155–169

Daux C, Moes N, Dolbow J, Sukumar N, Belytschko T (2000) Arbitrary branched and intersecting cracks with the extended finite element method. Int J Numer Methods Eng 48:1741–1760

Eischen JW (1987) An improved method for computing the J2 integral. Eng Fract Mech 26:691–700

Erdogan F, Gupta GD, Ratwani M (1974) Interaction between a circular inclusion and an arbitrarily oriented crack. J Appl Mech 41:1007–1013

Eshelby JD (1957) The determination of the elastic field of an ellipsoidal inclusion, and related problems. Proc R Soc Lon Ser A 241:376–396

Faber KT, Evans AG (1983a) Crack deflection processes. 1. Theory. Acta Metall Mater 31:565–576

Faber KT, Evans AG (1983b) Crack deflection processes. 2. Experiment. Acta Metall Mater 31:577–584

Gdoutos EE (1985) Stable growth of a crack interacting with a circular inclusion. Theor Appl Fract Mech 3:141–150

Gomez S, He W (2006) Laboratory method to evaluate fracture development in hard shale formations exposed to drilling fluids. In: Paper presented at the AADE 2006 fluids conference, Houston, April 11–12

Gramberg J (1965) The axial cleavage fracture 1 Axial cleavage fracturing, a significant process in mining and geology. Eng Geol 1:31–72

Gupta M, Alderliesten RC, Benedictus R (2015) A review of T-stress and its effects in fracture mechanics. Eng Fract Mech 134:218–241

Haddi A, Weichert D (1998) Three-dimensional interaction between a crack front and particles. Int J Numer Methods Eng 42:1463–1476

Han JJ, Chen YH (2000) T-effect for the interaction problem of an interface macrocrack with a near-tip microvoid. Int J Fract 102:205–222

Hassoun J, Derrien G, Panero S, Scrosati B (2008) A nanostructured Sn–C composite lithium battery electrode with unique stability and high electrochemical performance. Adv Mater 20:3169–3175

Herrmann AG, Herrmann G (1981) On energy-release rates for a plane crack. J Appl Mech 48:525–528

Hwu CB, Liang YK, Yen WJ (1995) Interactions between inclusions and various types of cracks. Int J Fract 73:301–323

Kitey R, Tippur HV (2005a) Role of particle size and filler-matrix adhesion on dynamic fracture of glass-filled epoxy. I. Macromeasurements. Acta Mater 53:1153–1165

Kitey R, Tippur HV (2005b) Role of particle size and filler-matrix adhesion on dynamic fracture of glass-filled epoxy. II. Linkage between macro- and micro-measurements. Acta Mater 53:1167–1178

Kitey R, Tippur HV (2008) Dynamic crack growth past a stiff inclusion: optical investigation of inclusion eccentricity and inclusion-matrix adhesion strength. Exp Mech 48:37–53

Kitey R, Phan AV, Tippur HV, Kaplan T (2006) Modeling of crack growth through particulate clusters in brittle matrix by symmetric-Galerkin boundary element method. Int J Fract 141:11–25

Knight MG, Wrobel LC, Henshall JL, De Lacerda LA (2002) A study of the interaction between a propagating crack and an uncoated/coated elastic inclusion using the BE technique. Int J Fract 114:47–61

Kumar R, Woo JH, Xiao XC, Sheldon BW (2017) Internal microstructural changes and stress evolution in silicon nanoparticle based composite electrodes. J Electrochem Soc 164:A3750–A3765

Lei J, Wang YS, Gross D (2005) Analysis of dynamic interaction between an inclusion and a nearby moving crack by BEM. Eng Anal Bound Elem 29:802–813

Li RS, Chudnovsky A (1993a) Energy analysis of crack interaction with an elastic inclusion. Int J Fract 63:247–261

Li RS, Chudnovsky A (1993b) Variation of the energy-release rate as a crack approaches and passes through an elastic inclusion. Int J Fract 59:R69–R74

Li Q, Lv JN (2017) Invariant integrals of crack interaction with an inhomogeneity. Eng Fract Mech 171:76–84

Li ZH, Yang LH (2004) The near-tip stress intensity factor for a crack partially penetrating an inclusion. J Appl Mech 71:465–469

Lipetzky P, Knesl Z (1995) Crack-particle interaction in a two-phase composite. 2. Crack deflection. Int J Fract 73:81–92

Lipetzky P, Schmauder S (1994) Crack-particle interaction in 2-phase composites. 1. Particle-shape effects. Int J Fract 65:345–358

Moes N, Dolbow J, Belytschko T (1999) A finite element method for crack growth without remeshing. Int J Numer Methods Eng 46:131–150

Mura T (1987) Micromechanics of defects in solids, 2nd edn. Martinus Nijho Publishers, Dordrecht

Muthu N, Falzon BG, Maiti SK, Khoddam S (2013) Modelling crack propagation in particle-reinforced composites using the element-free Galerkin method. In: Paper presented at the 19th international conference on composite materials, Montreal, July 28–August 2

Muthu N, Maiti SK, Falzon BG, Yan WY (2016) Crack propagation in non-homogenous materials: evaluation of mixed-mode SIFs, T-stress and kinking angle using a variant of EFG method. Eng Anal Bound Elem 72:11–26

Nielsen CV, Legarth BN, Niordson CF (2012) Extended FEM modeling of crack paths near inclusions. Int J Numer Methods Eng 89:786–804

Obrovac MN, Chevrier VL (2015) Alloy negative electrodes for Li-ion batteries (vol 114, pg 11444, 2014). Chem Rev 115:2043–2043

Ponnusami SA, Turteltaub S, van der Zwaag S (2015) Cohesive-zone modelling of crack nucleation and propagation in particulate composites. Eng Fract Mech 149:170–190

Rubinstein AA (1991) Mechanics of the crack path formation. Int J Fract 47:291–305
Sendeckyj GP (1974) Interaction of cracks with rigid inclusions in longitudinal shear deformation. Int J Fract 10:45–52
Sherry AH, France CC, Goldthorpe MR (1995) Compendium of T-Stress solutions for 2 and 3-dimensional cracked geometries. Fatigue Fract Eng Mater Struct 18:141–155
Tamate O (1968) The effect of a circular inclusion on the stresses around a line crack in a sheet under tension. Int J Fract Mech 4:257–266
Wang YB, Chau KT (2001) A new boundary element method for mixed boundary value problems involving cracks and holes: interactions between rigid inclusions and cracks. Int J Fract 110:387–406
Wang C, Libardi W, Baldo JB (1998) Analysis of crack extension paths and toughening in a two phase brittle particulate composite by the boundary element method. Int J Fract 94:177–188
Wang ZY, Ma L, Wu LZ, Yu HJ (2012) Numerical simulation of crack growth in brittle matrix of particle reinforced composites using the XFEM technique. Acta Mech Solida Sin 25:9–21
Wang ZY, Yu HJ, Wang ZH (2015) A local mesh replacement method for modeling near-interfacial crack growth in 2D composite structures. Theor Appl Fract Mech 75:70–77
Wang ZY, Gu J, Hou C, Song M (2018) Numerical simulation of the interaction between a crack and an inclusion: the role of T-stress for 2D composite materials. Multidiscip Model Mater Struct 14:339–359
Williams ML (1957) On the stress distribution at the base of a stationary crack. J Appl Mech 24:109–114
Zhou C, Li ZH (2007) The effect of T-stress on crack-inclusion interaction under mode I loading. Mech Res Commun 34:283–288
Zhou R, Li Z, Sun J (2011) Crack deflection and interface debonding in composite materials elucidated by the configuration force theory. Compos Part B Eng 42:1999–2003